



Functional stability of water wire–carbonyl interactions in an ion channel

Joana Paulino^a, Myunggi Yi^b, Ivan Hung^a, Zhehong Gan^a, Xiaoling Wang^{a,1}, Eduard Y. Chekmenev^{c,d,e,f}, Huan-Xiang Zhou^{g,h}, and Timothy A. Cross^{a,i,j,2}

^aNational High Magnetic Field Laboratory, Tallahassee, FL 32310; ^bDepartment of Biomedical Engineering, Pukyong National University, 48513 Busan, South Korea; ^cDepartment of Chemistry, Wayne State University, Detroit, MI 48201; ^dKarmanos Cancer Institute, Wayne State University, Detroit, MI 48201; ^eIntegrative Biosciences, Wayne State University, Detroit, MI 48201; ^fRussian Academy of Sciences, 119991 Moscow, Russia; ^gDepartment of Chemistry, University of Illinois at Chicago, Chicago, IL 60607; ^hDepartment of Physics, University of Illinois at Chicago, Chicago, IL 60607; ⁱDepartment of Chemistry & Biochemistry, Florida State University, Tallahassee, FL 32306; and ^jInstitute of Molecular Biophysics, Florida State University, Tallahassee, FL 32306

Edited by G. Marius Clore, National Institute of Diabetes and Digestive and Kidney Diseases, National Institutes of Health, Bethesda, MD, and approved April 10, 2020 (received for review January 19, 2020)

Water wires are critical for the functioning of many membrane proteins, as in channels that conduct water, protons, and other ions. Here, in liquid crystalline lipid bilayers under symmetric environmental conditions, the selective hydrogen bonding interactions between eight waters comprising a water wire and a subset of 26 carbonyl oxygens lining the antiparallel dimeric gramicidin A channel are characterized by ¹⁷O NMR spectroscopy at 35.2 T (or 1,500 MHz for ¹H) and computational studies. While backbone ¹⁵N spectra clearly indicate structural symmetry between the two subunits, single site ¹⁷O labels of the pore-lining carbonyls report two resonances, implying a break in dimer symmetry caused by the selective interactions with the water wire. The ¹⁷O shifts document selective water hydrogen bonding with carbonyl oxygens that are stable on the millisecond timescale. Such interactions are supported by density functional theory calculations on snapshots taken from molecular dynamics simulations. Water hydrogen bonding in the pore is restricted to just three simultaneous interactions, unlike bulk water environs. The stability of the water wire orientation and its electric dipole leads to opposite charge-dipole interactions for K⁺ ions bound at the two ends of the pore, thereby providing a simple explanation for an ~20-fold difference in K⁺ affinity between two binding sites that are ~24 Å apart. The ¹⁷O NMR spectroscopy reported here represents a breakthrough in high field NMR technology that will have applications throughout molecular biophysics, because of the acute sensitivity of the ¹⁷O nucleus to its chemical environment.

molecular dynamics | gramicidin A | ultra-high field NMR | water wire | ¹⁷O NMR

Water plays a crucial role in facilitating the structural flexibility and chemistry of proteins (1–5). For some proteins, this flexibility and chemistry are attributed to a string of hydrogen-bonded water molecules known as a water wire, as in potassium channels, aquaporins, and gramicidin A (gA) (6–9). In the latter case, a water wire mediates the transport of protons and other monovalent cations across cellular membranes (10). Many novel materials also utilize water wires, including carbon nanotubes (11), a self-assembled imidazole I quartet superstructure with potential applications for desalination (12), and a bole-amphiphile-triazole compound that undergoes self-assembly to form pores analogous to gramicidin A (gA) (13). Discovered in 1939 (14), gA was the first antibiotic to be used clinically and continues to be used today to treat certain eye infections (15). The antimicrobial activity derives from its ability to form a transmembrane channel that is selective for monovalent cations.

gA forms a β-strand of alternating D- and L-amino acids wound into a right-handed helical structure with 6.3 residues per turn. The alternating chirality of the amino acids results in the side chains being on one side of the β-strand facing the fatty acyl chains of the membrane environment while the peptide planes line an aqueous pore (*SI Appendix, Fig. S1*). The all atom

high-resolution dimeric structure was characterized from oriented sample solid-state NMR (OS ssNMR) spectroscopy in lipid bilayers (16, 17). Solution NMR in detergent micelle environments has also shown the same hydrogen-bonding pattern for the backbone structure lining the pore (18, 19). In a lipid bilayer, gA forms an N terminus-to-N terminus dimer, with the formylated (F) N termini at the center of the bilayer (20). The C termini are capped with ethanolamine; the outermost even-numbered carbonyls L14, L12, and L10 in each subunit form the channel entrance and facilitate the dehydration of cations in a stepwise process (21). These three sites are exposed to a successively decreasing number of waters, with L10 typically interacting with three waters. The ¹⁵N OS ssNMR studies with single occupancy K⁺ showed very small structural perturbations and, even with double occupancy, only minor structural perturbations at the mouth of the pore. The maximal effect was observed at the W13 ¹⁵N backbone site in the peptide plane, with the L12 carbonyl resulting in a maximal structural perturbation of just 4° (21). In the analysis presented here for ¹⁷O OS ssNMR, the perturbations of the pore lining residues were dominated not by minor structural effects, but by a dramatic influence of selective hydrogen bonding on the quadrupolar interaction. The single file

Significance

Despite the well-characterized structural symmetry of the dimeric transmembrane antibiotic gramicidin A, we show that the symmetry is broken by selective hydrogen bonding between eight waters comprising a transmembrane water wire and a specific subset of the 26 pore-lining carbonyl oxygens of the gramicidin A channel. The ¹⁷O NMR spectroscopic resolution of the carbonyl resonances from the two subunits required the use of a world record high field magnet (35.2 T; 1,500 MHz for ¹H). Uniquely, this result documented the millisecond timescale stability of the water wire orientation within the gramicidin A pore that had been reported to have only subnanosecond stability. These ¹⁷O spectroscopic results portend wide applications in molecular biophysics and beyond.

Author contributions: J.P., I.H., Z.G., E.Y.C., H.-X.Z., and T.A.C. designed research; J.P., M.Y., I.H., Z.G., X.W., and E.Y.C. performed research; J.P., M.Y., I.H., H.-X.Z., and T.A.C. analyzed data; and J.P., Z.G., H.-X.Z., and T.A.C. wrote the paper.

The authors declare no competing interest.

This article is a PNAS Direct Submission.

This open access article is distributed under [Creative Commons Attribution-NonCommercial-NoDerivatives License 4.0 \(CC BY-NC-ND\)](https://creativecommons.org/licenses/by-nc-nd/4.0/).

¹Present address: Department of Chemistry and Biochemistry, University of California, Santa Barbara, CA 93106.

²To whom correspondence may be addressed. Email: cross@magnet.fsu.edu.

This article contains supporting information online at <https://www.pnas.org/lookup/suppl/doi:10.1073/pnas.2001083117/-DCSupplemental>.

aqueous pore, terminated by the two L10 carbonyls, is only wide enough to host a single file of hydrogen-bonded water molecules: i.e., a water wire, as well as various monovalent cations ranging from Li^+ to Cs^+ . The peptide planes of gA are nearly parallel to the pore axis, with odd-numbered carbonyls in both subunits oriented toward the bilayer center and even-numbered carbonyls toward the bilayer surfaces. Upon entering the water wire region of the channel, a cation interacts with only two waters and possibly pairs of carbonyl oxygens following a spiral path through the pore (21).

The potential of ^{17}O NMR for elucidating functional understanding of biological chemistry has long been recognized (22–34). Preliminary results from ^{17}O -labeled L10, L12, and L14 in the presence of double occupancy K^+ have been reported using low field spectroscopy showing that ^{17}O spectroscopy would be a much more sensitive tool for such studies than ^{15}N spectroscopy (34). The site-specific labeling of gA carbonyl oxygens permitted acquisition of high-resolution data from individual atomic sites interacting with the water wire in the pore and with cations at the opposite ends of the pore. However, the low-gyromagnetic ratio of ^{17}O , its quadrupole moment, and resulting broad spectral resonances make ^{17}O NMR spectroscopy challenging. Here, we overcame this challenge by acquiring ^{17}O OS ssNMR spectra at 35.2 T (1,500 MHz for ^1H and 203 MHz for ^{17}O), a field strength 25% higher than the highest commercially available NMR spectrometers (28.1 T or 1,200 MHz for ^1H). The results reveal that selective pore-lining carbonyl oxygens form remarkably stable hydrogen bonds with waters in the wire, such that the water wire does not change its orientation on the millisecond NMR timescale. The stable orientation of the water-wire dipole also provides a simple explanation for the low affinity of the second cation binding site in this dimeric channel, despite a separation of $\sim 24 \text{ \AA}$ from the first binding site at the opposite end of the pore. The ^{17}O NMR spectroscopy reported here represents a breakthrough in ultra-high field NMR technology that will have applications throughout molecular biophysics, because of the acute sensitivity of the ^{17}O nucleus to its chemical environment (32–34).

Results

The antiparallel dimeric symmetry of the gA structure has been extensively documented in lipid bilayer environments, as well as in detergent-based membrane mimetic environments (Protein Data Bank [PDB] ID codes 1NRM, 1JNO, 1MAG, and 1GRM) (18, 19, 35). As further support of this symmetry, ^{15}N OS ssNMR spectra were acquired at 35.2 T. Slices through the ^{15}N anisotropic chemical shift and ^1H - ^{15}N dipolar coupling dimensions of a two-dimensional (2D) spectrum obtained from a uniformly oriented sample are shown in Fig. 1 (36), along with a gA structure illustrating the ^{15}N -labeled sites. Importantly, the single dipolar coupling and chemical shift peaks for each labeled site document with high precision the structural symmetry of the two subunits in the transmembrane dimer. The very narrow line widths (1.5 to 2.0 parts per million [ppm]) of the chemical shift resonances relative to the chemical shift anisotropies of 169 ppm for G2 and 175 ppm for A3, and the narrow line widths of the ^1H - ^{15}N dipolar couplings, which report on the N–H bond orientation with respect to the gA channel axis, define the bond orientations with a very small imprecision of less than 2.0° , for the orientation of the peptide planes containing the two ^{15}N sites (37). These narrower line widths in the current spectra compared to the Mai et al. spectra obtained at 4.7 T (37) are in part due to an enhanced alignment of the samples at the much higher magnetic field strength. It is also important to note that these data are within the error bars of those reported 26 y ago (16, 37). The dipolar couplings and anisotropic chemical shifts determined here are very similar to those determined previously: $21.4 \pm 0.4 \text{ kHz}$ and $222.6 \pm 1 \text{ ppm}$ (vs. 21.8 kHz and 224 ppm in

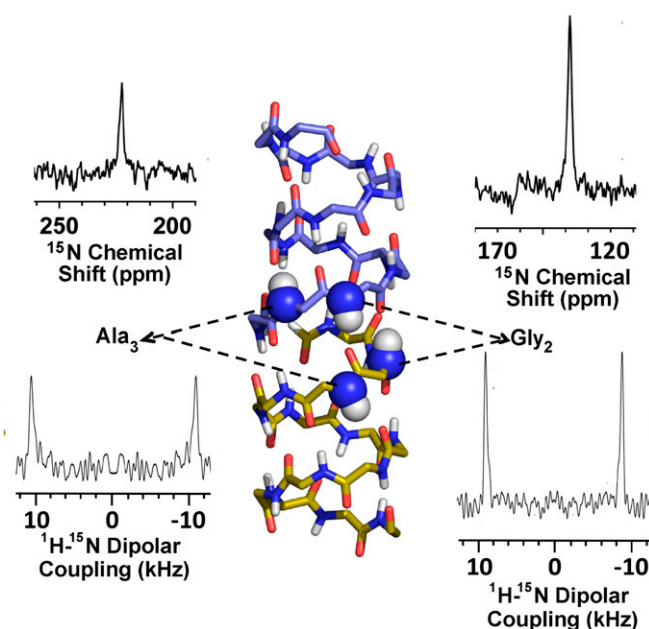


Fig. 1. Slices through the ^1H - ^{15}N dipolar and ^{15}N anisotropic chemical shift dimensions of the 2D OS ssNMR (SAMPI4) spectra of ^{15}N G2- and ^{15}N A3-labeled gA at 35.2 T (36), showing excellent alignment of gA in liquid-crystalline lipid bilayers of DMPC and precise dimeric symmetry of the structure. The gramicidin structure is a dimer (upper monomer carbon is light blue and nitrogen dark blue; lower monomer carbon is gold and nitrogen dark blue). Oxygen is red and hydrogen is white. This illustrates the two ^{15}N - ^1H sites in each subunit (dark blue and white spheres) that were ^{15}N -labeled for this OS ssNMR sample in the liquid-crystalline preparation. The spectrum of the two A3 sites is shown on the left and the two G2 sites on the right.

1993) for the A3 ^{15}N site and $17.8 \pm 0.6 \text{ kHz}$ and $137.5 \pm 1.5 \text{ ppm}$ (vs. 17.6 kHz and 139 ppm in 1993) for the G2 site. *SI Appendix, Figs. S2 and S3, Table S1, and Supplementary Information Text* present additional data demonstrating the dimeric symmetry of the gA structure in the same lipid bilayer environment as used in this study. Furthermore, the symmetry of the antiparallel gA structure mimics the “antiparallel” symmetry of the lipid bilayer environment. Indeed, based on the ^{15}N data and the lipid environment, there is no expectation that the structure should be anything but symmetric.

Prior OS ssNMR spectra of single site ^{17}O -labeled gA at lower fields (19.6 and 21.1 T) showed single broad ($\sim 30 \text{ ppm}$) resonances even in the presence of ^1H decoupling (24, 34), but, at the higher field of 35.2 T, the ^{17}O line widths are reduced by more than a factor of two due to increased alignment and reductions in the second-order quadrupolar shielding and T_2 relaxation line width in units of ppm (*SI Appendix, Fig. S4*) (38, 39). This permits resolution of the two ^{17}O resonances for each of three labeled carbonyl sites in the gramicidin dimer (Fig. 2). ^{17}O peak positions which are sums of the chemical and second-order quadrupolar shifts are dominantly determined by the chemical shift term at the 35.2-T field. The other two ^{17}O -labeled carbonyl sites are in the final turn of the helical structure at the membrane interface exposed to the bulk aqueous environment. Each of these interfacial sites displays a single resonance, resulting from an averaged environment due to rapid hydrogen bond exchange with the bulk aqueous environs. In addition, these two resonances are shifted upfield, reflecting increased peptide plane dynamics and hydrogen bonding with water in the final turn of the structure. A similar averaging of the anisotropy was previously observed for amide ^{15}N OS ssNMR resonances in the last turn of the helix (37). G2 and L4 ^{17}O resonances are downfield

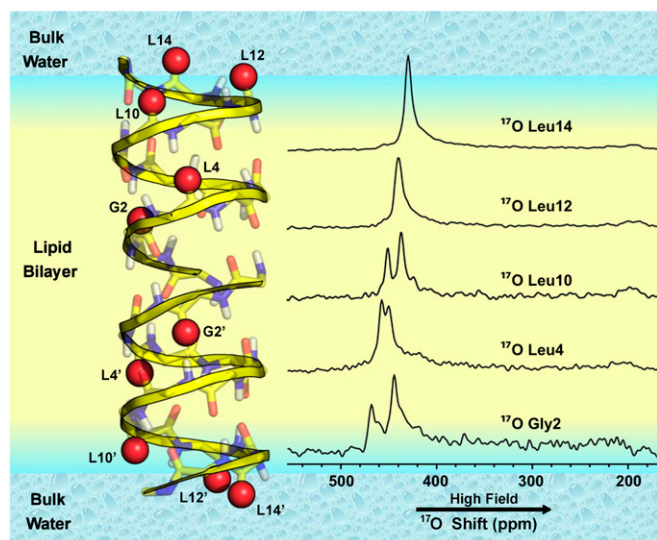


Fig. 2. ^{17}O OS ssNMR of gA dimer in liquid-crystalline lipid bilayers at 35.2 T. G2, L4, L10, L12, and L14 were individually labeled with ^{17}O such that each sample was labeled in both gA subunits with the same isotopically labeled amino acid residue as shown in the structural model. The two subunits are distinguished here with residue labels primed in one subunit and unprimed in the other subunit. The ^1H decoupled spectra show single resonances for L12 and L14 and two resonances for each of the other three sites: G2, L4, and L10. The colors in the structure are explained in Fig. 1.

relative to the L10, -12, and -14 counterparts because these peptide planes are each stabilized with hydrogen bonds to pairs of adjacent peptide planes (37). The L10 carbonyl peptide plane is likely hydrogen bonded to the ethanolamine C-terminal blocking group for at least a portion of the time, generating an intermediate shift.

Two Resonances for Sites Lining the Pore. Notably, the ^{17}O OS ssNMR spectra for G2, L4, and L10 each show a pair of resonances, which suggest the existence of two distinct chemical environments for each of their carbonyl oxygens. An analysis of the spectral intensities of the well-resolved G2 and L10 resonance pairs is presented in *SI Appendix, Fig. S5*, showing approximately equal intensities for the two resonances in each pair. Previously, all of the gA structures that support a cation-conducting pore have demonstrated dimeric symmetry as discussed above. Indeed, no evidence for asymmetry either in the polypeptide backbone or in the side chains has been reported by solution or ssNMR spectroscopy (16–19, 36). Likewise, X-ray structures from lipidic cubic phase and organic solvents that stabilize nonconducting intertwined double helical structures are all symmetric dimers (40–42). Furthermore, the very high resolution of the ^{15}N data shown in Fig. 1 presents the strongest evidence for structural equivalence between the two subunits. If the pairs of ^{17}O resonances were interpreted as structural differences, the predicted ^{15}N anisotropic chemical shifts and ^{15}N - ^1H dipolar couplings could not be reconciled with the experimental data (*SI Appendix, Fig. S6*).

Even for a dimer with the same structure, asymmetry can arise from differences in the chemical environment in the pore. Specifically, a water wire that forms an electric dipole extending the full length of the pore, as shown by molecular dynamics (MD) simulations (43, 44), if stably oriented on the NMR timescale, could break the antiparallel symmetry of the gA subunits (Fig. 3A). Hydrogen bonding to selective backbone carbonyl oxygens from the water wire could lead to inequivalent chemical

environments for the two subunits and hence a pair of resonances for each labeled site, as detected here for the carbonyl ^{17}O resonances from G2, L4, and L10 in the two subunits. Moreover, we note that ^{17}O spectroscopy is particularly sensitive to hydrogen bonding (25, 26, 32, 33, 45–49). Indeed, through the ^{17}O quadrupolar interaction, it is entirely possible to explain the observed ^{17}O resonance frequencies solely by differences in the interaction strength with the water wire: i.e., without the need for altering the structural symmetry of the dimer, as described in detail below.

The ^{17}O spectra of the six labeled pore-lining carbonyls indicate that the magnitude of the influence by the chemical environments varies not only from one subunit to the other, but also from one site to another within a subunit, such that, for G2 and L10, nearly baseline resolution is observed while, for L4, the two resonances are barely resolved. To understand these differences, we note that a single file of eight waters, with an average spacing of ~ 2.85 Å between nearest neighbors, extends through the gA pore over a total length of 20 Å, slightly greater than the 19.2-Å separation of the two L10 carbonyl oxygens in the dimer. With one proton in each water molecule projected axially to form the water wire, only eight protons from the water wire project equatorially to potentially hydrogen bond with a selection of the 28 gA carbonyls lining the pore between and including the L10 sites. Some of these carbonyls may be in an optimal position for a stable hydrogen bond with water, others may compete with adjacent sites for hydrogen bonding to the same water, and still others may have little chance for hydrogen bonding to waters.

For the water wire to induce observable differences in the ^{17}O shifts (where “shifts” refer to the combination of chemical and quadrupolar components that comprise the ^{17}O resonances) between the two subunits, these hydrogen bonding interactions with water must be stable for a period of time greater than the inverse of the separation between the two observed ^{17}O resonances in units of hertz. For L4, the separation of the frequencies is 1.4 kHz; for G2, it is 4.7 kHz; and, for L10, it is intermediate at 2.8 kHz. These observations consequently require the lifetime of the water wire orientation to be longer than 0.7 ms; otherwise, exchange between the water hydrogen bonded and nonhydrogen bonded states will result in averaging of the resonance frequencies, as shown by the L12 and L14 resonances through their rapid exchange with the bulk water. Raising the temperature should shorten the lifetime of the water wire orientation. *SI Appendix, Fig. S7* displays a comparison of data obtained at 30 °C and 52 °C for the L10-labeled site, showing that the spectra are superimposable. Hence, there is no sign that raising the temperature to 52 °C shortens the observed lifetime of the water wire orientation, suggesting that the stability of the water wire at 30 °C is greater than 0.7 ms.

We investigated carbonyl–water hydrogen bonding interactions by MD simulations. The simulations showed the gA pore filled with a single file of eight ordered water molecules and that the lifetime of the electric dipole orientation of the water wire in these simulations was on the order of 0.1 ns. The O–O separation of ~ 2.85 Å between adjacent water molecules is similar to the carbonyl O–O separation of ~ 3.1 Å along the pore axis between i and $i + 4$ carbonyls in a subunit. For example, the L10 and G2 carbonyls match the water positions (Fig. 3) reasonably well, resulting in hydrogen bonds with water protons from the first and third waters in the water wire, but not for the isotopically labeled L4. Instead it is the unlabeled V6 site that would be in a position to hydrogen bond with the second water. After G2, the mismatch in position between the water protons and the carbonyl oxygens accumulates along the pore axis, resulting in different hydrogen bonding options for the waters in the second gA subunit (designated with a prime). Specifically, the fourth water may hydrogen bond with A3 or V1', the fifth

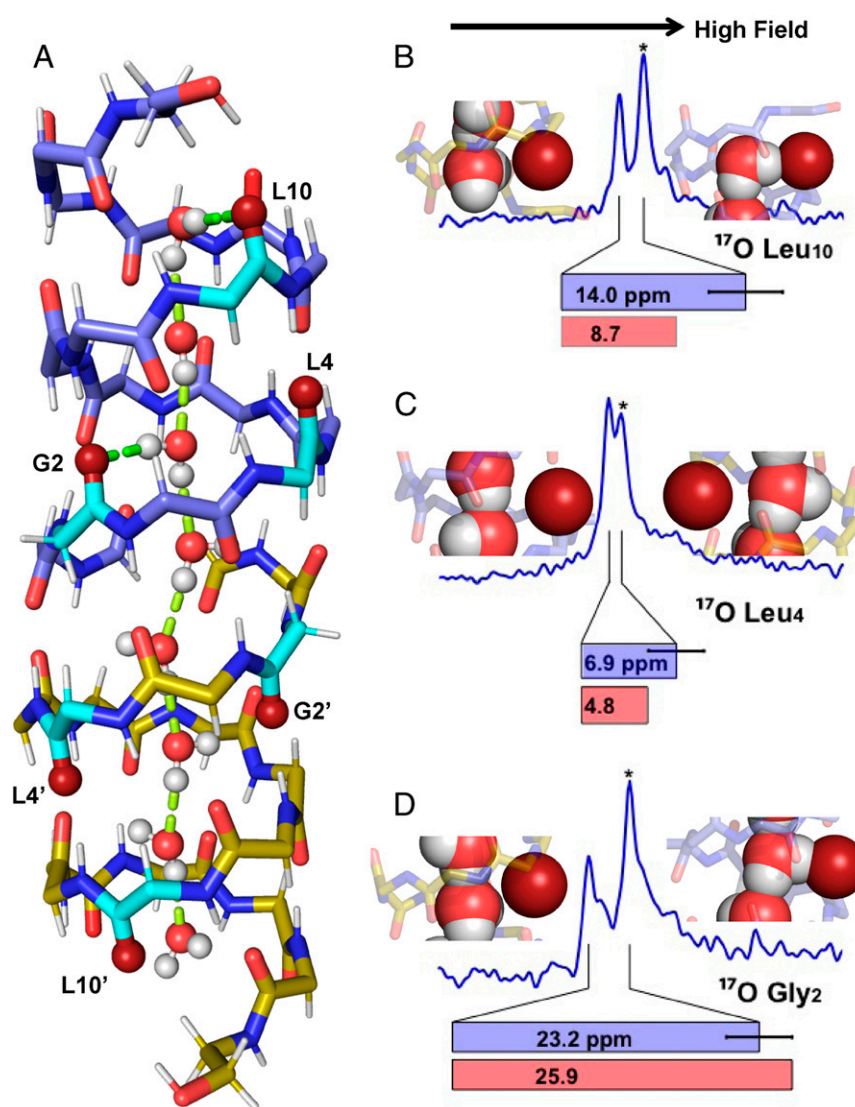


Fig. 3. (A) MD snapshot of a water wire, placed in the 1MAG structure and optimized by DFT, showing hydrogen bonding between the water wire and L10 and G2 carbonyls of the upper subunit (bright green) as well as hydrogen bonding between water molecules (pale green). Colors of atoms as in Fig. 1 except that the ^{17}O -labeled peptide planes are colored in turquoise. L4 does not receive a hydrogen bond while L4' appears to be in a position to receive a weak hydrogen bond. (B–D) Observed ^{17}O spectral resonances for the L10 (B), L4 (C), and G2 (D) ^{17}O (blue). The resonances marked (*) are shifted upfield by hydrogen bonding with water. Also shown are DFT calculations of the ^{17}O frequency shift difference between the two subunits (red bars) compared to the observed shift difference (blue bars). Water interactions with these six carbonyl oxygens in the DFT optimized structure are shown with individual carbonyl oxygens (deep red) interacting or not interacting with water molecules..

water with the formyl' (F') or A5', the sixth water with L4' or W9', the seventh with V8' or W13', and the eighth with L10' or W15'.

We then quantified the influence of hydrogen bonding between the waters and carbonyl oxygens on the carbonyl ^{17}O shifts by density functional theory (DFT) calculations. We chose a snapshot of a typical continuous water wire from MD simulations, replaced the channel with the symmetric gA structure (PDB ID code 1MAG), and optimized the geometry by DFT prior to NMR chemical shift calculations (Fig. 3A). The carbonyl oxygen shifts calculated by DFT for the G2, G2', L4, L4', L10, and L10' sites have differences between the subunits that agree well with the experimental data (Fig. 3B–D). Hence, we are in a position to make assignments for the resonances of the labeled sites. Both the G2 and L10 carbonyls (in the first subunit) have stable hydrogen bonding with waters near the negative end of the electric dipole while G2' and L10' (in the second subunit) have

very limited opportunities for hydrogen bonding. Of the pairs of resonances from the G2- and G10-labeled samples, the upfield ones belong to G2 and G10 in the first subunit (Fig. 3B and D). The upfield shift of the ^{17}O resonances upon hydrogen bonding is well-documented in the literature for model systems (25, 26, 32, 33, 45–49). The uniformity of the hydrogen bonded and nonhydrogen bonded populations is clear for these sites by the equivalent spectral intensities, as simulated in *SI Appendix*, Fig. S5.

The situation is very different for the L4-labeled sample. First, the upfield resonance belongs to L4' in the second subunit, which, as mentioned above, has the possibility to hydrogen bond with the sixth water (Fig. 3C). Second, the upfield shift of the L4' resonance is relatively small, consistent with the DFT calculation, suggesting nonoptimal geometry when the L4'–water hydrogen bond does form. Third, the intensity of the upfield L4' resonance is clearly not equal to that of the downfield L4

resonance. We interpret the unequal intensities as indicating that L4' has two populations: the one where the L4'–water hydrogen bond does form, giving rise to the upfield resonance, and the other where this hydrogen bond does not form, giving rise to a downfield resonance that merges with the L4 resonance. The result is a significant intensity difference between the two resonance frequencies. Note that the population heterogeneity of the L4' site has to be stable on the millisecond timescale as rapid exchange would lead to a resonance with intensity equal to that of the L4 resonance.

Importantly, the ^{15}N OS ssNMR data (Fig. 1 and *SI Appendix*, Fig. S2), which are particularly sensitive to the orientation of the peptide planes in the gramicidin backbone, show no distinction between these two subunits. Specifically, the A3 amide site is part of the same peptide plane as the G2 carbonyl. Changes in the dynamic average of the peptide plane tilt angles of even 1° to 2° can be detected by such spectra. The lack of structural distortion induced by hydrogen bonding with water is due to the fact that the waters in the water wire can shift their position within the narrow pore toward the carbonyl oxygens without disrupting the hydrogen bonding between the water molecules and without inducing a structural change in the backbone.

It is clear, in all of the MD simulations, that there is a preference for specific water–carbonyl hydrogen bonds; however, the modeled lifetimes (subnanosecond) of these interactions, which are largely independent of the water models used (*SI Appendix*, Fig. S8), are significantly shorter than the lifetimes (millisecond) observed by the ^{17}O NMR spectral results. The water models, such as TIP3P and SPC, in classical MD simulations, have been optimized to reproduce the properties of bulk water (with an average of ~ 3.6 hydrogen bonds per water). However, in the pore, the water molecules are not bulk-like but are restricted to a maximum of three hydrogen bonds per water—two of those bonds are with adjacent waters, and the third is with a carbonyl oxygen. Therefore, it may not be very surprising that the stability of the water wire in gA is not optimally modeled by these water models. Recent ab initio MD simulations have shown that, while interacting with a chloride ion, the water dipole flips rapidly on the picosecond timescale, but, with a fluoride ion where the proton approaches more closely, the water dipole becomes stable (50). This work hints that a quantum treatment of the water wire in the gA pore, where waters are restricted in orientation to form strong interactions with carbonyls, may have a much longer lifetime than in the classical MD simulations. Still, the MD simulations sampled configurations that illustrate experimentally implicated hydrogen bonds.

Influence of Cation Binding. The L10, -12, and -14 carbonyl sites at either end of the pore have been hypothesized to take part in a stepwise dehydration of cations prior to their passage through the pore, solvated only by the waters of the water wire and carbonyl oxygens lining the pore (21). The energetic cost associated with cation dehydration increases with each water that is removed, and, consequently, the two most costly waters remain on the cation as it transits the pore. The spectra of ^{17}O -labeled gA for two concentrations of K^+ ions associated with single (0.07 M salt) and double occupancy (2.4 M salt) of the gA channel are compared in Fig. 4 to those without cations. Single-occupancy cation binding influences sites in the direct vicinity of the cation binding site, the L10 and L12 carbonyl oxygens, but not the L14 or the G2 and G2' sites labeled here (21). The implication is that, once the third water is removed from the cation hydration sphere, the cation is free to transit through the pore, a process that is rapid. With single K^+ occupancy, the cation further stabilizes the negative end of the water-wire electric dipole. The lack of change in the G2/G2' spectra upon K^+ single occupancy confirms the stability of the water positions in the pore, even in the absence of ion binding. This suggests that the

water–carbonyl interactions throughout much of the channel are unperturbed by single-occupancy K^+ binding (21).

The two resonances of L10 under conditions of single cation occupancy show small upfield shifts of 7 and 12 ppm. Since cation binding involves L10, a modest shift was anticipated for this site by direct interaction with the cation while a shift for the distal L10' suggests lengthening and/or further stabilization of the water wire due to strengthening of the electric dipole moment by cation binding at the opposite end of the pore. Furthermore, the L12 resonance that was a singlet in the cation-free sample splits into two resonances upon single occupancy, with one resonance shifted upfield and the other unshifted. This upfield-shifted resonance is assigned to L12 interacting with the cation. However, this resonance has a weak intensity, suggesting that, similar to the situation noted above for L4', the cation has two possible bound states: one where it directly interacts with both L12 and L10 and the other where it directly interacts only with L10. In the latter cation binding state, the L12 resonance merges with the L12' resonance, accentuating the disparity in intensity between the two frequencies. Note that the strengthening of the water wire induced by single ion occupancy and detected by L10' does not extend to the more distal L12' carbonyl oxygen site that shows no change in frequency upon single occupancy. This is not surprising since L12' has been modeled as having multiple waters from the bulk aqueous environment solvating this carbonyl oxygen (21).

Ion dissociation may be rapid on the millisecond timescale of the lifetime of the water wire orientation (51, 52). Dissociation (from the negative end of the water wire) is followed by rapid rebinding. Although rebinding by chance to the positive end of the water wire might flip the water wire orientation, rebinding to the negative end is favored by a factor of $\sim 20:1$, due to electrostatic attraction by the water-wire electric dipole (see below). This significant bias for the negative end means that ions can dissociate and rebind many times, and the water-wire orientation is still preserved.

At 2.4 M K^+ , the first ion binding site is fully occupied while the second (“low-affinity”) site has 80% occupancy. Unlike single occupancy that has a small effect on the anisotropy of the ^{17}O tensor, double occupancy results in a significant reduction of the ^{17}O anisotropy for the sites involved in cation binding, indicating enhanced carbonyl dynamics potentially associated with the exchange between L10 and L12 sites. These sites are also implicated by MD (Fig. 4), which also suggests that the low-affinity binding site is significantly off axis, permitting the water wire to have access to the bulk aqueous environment.

Clearly, cation binding in the high-affinity site significantly hinders K^+ binding in the low-affinity site. It is also clear, that K^+ double occupancy does not result in a symmetrized structure. Indeed, the water wire remains unidirectional throughout the pore, as in the single occupancy state. Small anisotropic ^{15}N chemical shifts ranging from 6 to 10 ppm have previously been detected only in the cation binding sites (i.e., W11, W13, and W15 corresponding to the peptide planes with L10, L12, and L14) under conditions of double occupancy.

With double occupancy there are many dramatic shifts in the ^{17}O resonances, presumably associated with the low-affinity subunit. The water wire appears to “tighten up” with slightly reduced water–water spacing, especially in the low-affinity subunit. Note that such packing is not restricted to an idealized z axis string of waters, but that there is a volume in this pore that can be optimally packed in response to the repulsion between the water-wire electric dipole and the ion at the low-affinity site. The sixth water in the wire now appears to be within range to hydrogen bond with the G2' carbonyl. This tightening of the water wire appears to have further optimized the geometry for the G2 hydrogen bond with the more stable third water, resulting in an additional upfield shift for this resonance.

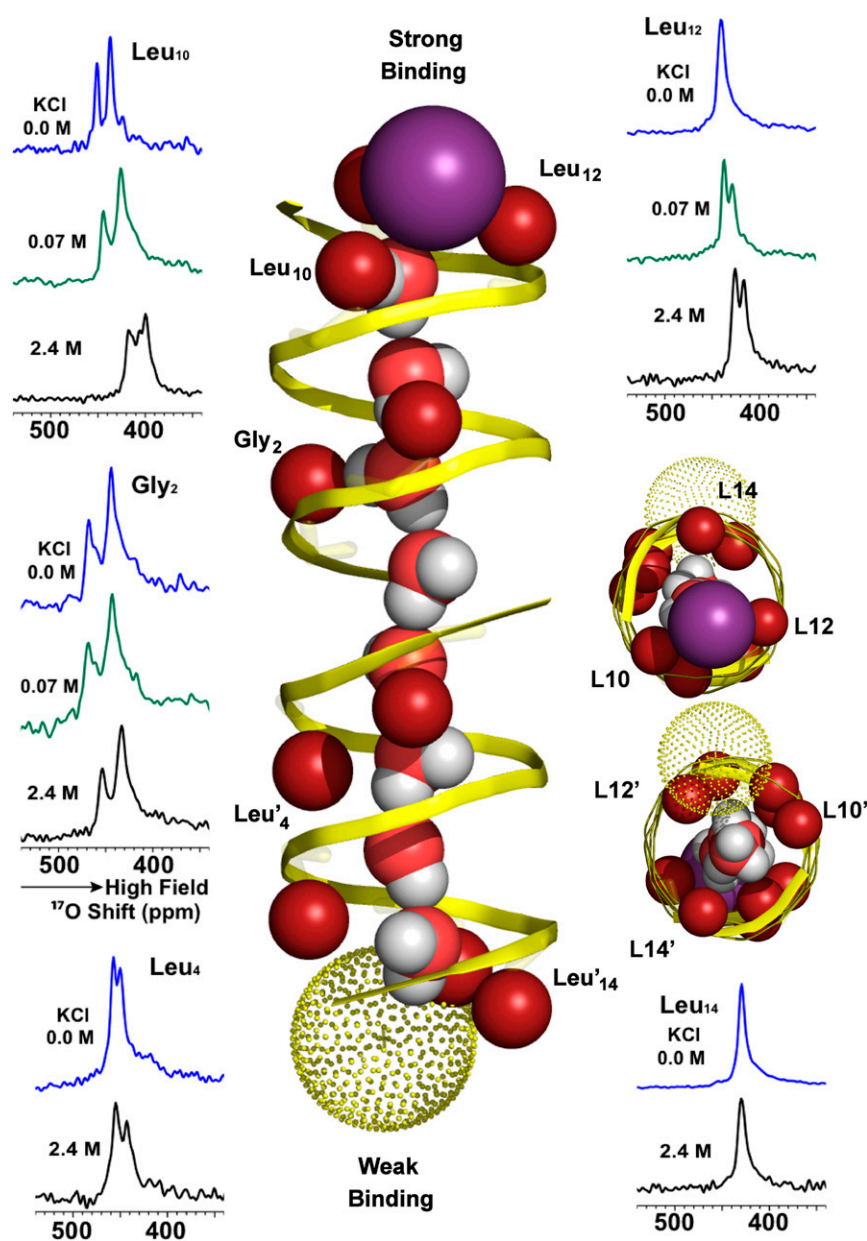


Fig. 4. ^{17}O OS ssNMR spectroscopy of ^{17}O single site labeled gA at G2, L4, L10, L12, and L14 in liquid-crystalline lipid bilayers with 0.0 M K^+ , 0.07 M K^+ , and 2.4 M K^+ (spectra for L4 and L14 at 0.07 M K^+ [green] were not recorded as only small differences were observed for their spectra at 0.0 [blue] and 2.4 M K^+ [black] ions). The high-affinity bound K^+ ion is illustrated as a purple sphere and the low-affinity K^+ ion as a yellow dotted sphere. The ion positions are based on previously published data (21) and the current study.

As mentioned above, an important feature of the electric dipole formed by the water wire observed in the MD simulations is its significant strength (12.1 ± 2.4 debye) that clearly influences cation binding at the low-affinity site, an example of negative cooperativity. Treating this dipole as continuously distributed over a line segment of 20-Å length (the distance between the two terminal molecules of the water wire), with the two ions at 2 Å from the terminal waters, and assuming an effective dielectric constant of 20, we estimate that the water-wire dipole would stabilize the high-affinity ion by 0.96 kcal/mol and destabilize the low-affinity ion by the same amount. The electrostatic interactions with a stable water-wire dipole would thus account for as much as an ~ 24 -fold difference in binding affinity, which is comparable to the experimentally measured ~ 20 -fold difference (21).

Discussion

The enhanced resolution of ^{17}O spectroscopy at a very high magnetic field reveals unique insights into the chemical interplay between a transmembrane channel, its aqueous environment, and cations. The exquisite sensitivity of this quadrupolar nucleus to delicate molecular interactions, such as hydrogen bonds with water, represents a unique scientific tool that is coming of age. Here, this technology has permitted experimental observation of selective hydrogen bonds between water wire protons and isotopically labeled carbonyl oxygens lining the gA channel pore. Furthermore, it has been possible to resolve the resonances and hence the hydrogen bonding interactions in each of the gA subunits, despite the identical peptide structures. In uniformly oriented liquid crystalline lipid bilayer samples the water-carbonyl interactions are shown to have at least millisecond lifetimes under

conditions with and without cations present when there is no cation or water concentration gradient across the membrane. Despite a relatively uniform distribution of the 28 carbonyl oxygens lining the pore, the hydrogen-bonding interactions with the eight water protons of the water wire are selective for specific carbonyl sites that are at an appropriate spacing along the water wire. The water wire itself has a stability gradient from the negative end of the electric dipole to the positive end, based on optimal hydrogen bonding of the waters at the negative end of the electric dipole. The water interactions at this end of the dipole over the first three waters of the water wire are particularly stable.

Water wires are critical biological assemblies supported by membrane proteins for the purposes of transporting charge and ions across membranes. The present unique high-resolution characterization of the gA water wire provides insights into the dynamics, structure, and functional mechanism of this ion channel. In liquid crystalline lipid bilayers, the gA water wire and its associated electric dipole are stable on the millisecond timescale, both with and without cations present. Upon single cation occupancy, the influence of the electric dipole extends even further into the terminal region of the second subunit than in the absence of cations. The K^+ interactions upon double occupancy do not result in symmetrization of the channel; however, there are significant impacts on water carbonyl interactions in the pore and hence on the resultant electric dipole that stabilizes the high affinity cation binding state. Furthermore, under double occupancy, the cations in the high- and low-affinity sites do not exchange sites at their respective ends of the channel on the millisecond timescale. Such exchange would flip the water wire and its associated electric dipole, resulting in averaging of the ^{17}O spectral frequencies of the two subunits into a single value. Consequently, these cation binding sites are also stable at least on the millisecond timescale. Indeed, the water-wire orientation and its associated electric dipole dictates the high-affinity and low-affinity sites of the dimer.

Utilizing the high-resolution structure of the gA channel derived in a lipid bilayer environment and the exquisite and well-documented sensitivity of ^{17}O carbonyl resonances to hydrogen bonding, the experimental results were coupled with MD to model the water-carbonyl interactions. DFT calculations supported the interpretation of the ^{17}O NMR resonance frequencies, generating a unique map of water/peptide interactions throughout the pore. In addition, ^{17}O carbonyl resonances of the pore in the presence of K^+ at single- and double-occupancy concentrations illustrated the influence of the cations on the water wire.

The profound influence of the water wire in this model system and the stable water-carbonyl interactions illustrate the significance and functionality for such wires in many channels and materials. In particular, the stability of the water wire and its electric dipole suggests that its influence in many other systems (6) could be more significant than generally recognized. To achieve such an understanding, unique ^{17}O spectroscopy as reported here at a field strength of 35.2 T demonstrates the exquisite sensitivity to the chemical environs surrounding oxygen sites where so much of biological chemistry takes place.

Materials and Methods

Sample Preparation. The ^{17}O enriched site specific labeled gA peptides utilized in this study had been previously synthesized and purified by Hu et al. (24). Briefly, amino acids were enriched by acid-catalyzed exchange at high temperature from $H_2^{17}O$ (70% ^{17}O enrichment; CIL, Andover, MA) as described by Steinschneider et al. (53). gA was synthesized by solid-phase peptide synthesis using the procedure described by Tian and Cross (21). In gA, the ^{17}O Leu labeling was determined to be 57% (24).

gA and dimyristoylphosphatidylcholine (DMPC) lipid (Avanti Polar Lipids) samples were prepared as previously described (54) via cosolubilization in trifluoroethanol (J.T. Baker) at a gA subunit-to-lipid molar ratio of 1:16. The solution was deposited on glass slides (Matsunami, Osaka, Japan), dried, and hydrated with 5 mM Tris buffer at pH 7.5 or KCl solutions (2.4 M and 0.07 M) at pH 7.0. Stacks of 40 to 42 slides were incubated for >36 h at 98% relative humidity (RH) and 37 °C prior to sealing and incubating at 37 °C. Final samples contained between 42% and 48% water by weight (55). We also note that the incubation of the sample in the presence of ions at 98% RH can add considerable water without cations to the sample.

NMR. Proton-decoupled ^{17}O solid state NMR spectra of specific site-labeled static gramicidin samples were acquired at 35.2 T (203 MHz) using a spin-echo sequence with $\pi/2$ and π pulse lengths of 1.5 μs and 3.0 μs , and a 20- μs echo period delay using an HX static probe at 30 °C (36). A 20-ms recycle delay period was used due to the 30-kHz proton decoupling. The length of signal averaging time was between 3 and 6 h for each of the spectra on the powered magnet (12 MW) that is operational for NMR on average ~100 h a month for 8 mo. Spectra of samples labeled at G2, L4, L12, and L14 were acquired using a DFS satellite-transition inversion pulse (56). SAMPI4 spectra and sample preparation for ^{15}N gA were described in ref. 36.

MD Simulation and Density Functional Theory Calculations. MD simulations of gA (PDB ID code 1MAG) were carried out using NAMD software (57) with CHARMM force field (58). The protein was solvated by a TIP3P pre-equilibrated DMPC lipid bilayer (59). After 10,000 steps of energy minimization, the system was gradually heated to 303 K for 60 ps under constant volume. The simulation system was equilibrated under constant pressure and temperature for 1 ns; all heavy atom restraints were removed, and the simulation continued for 792 ns. The nonbonded interactions were smoothly truncated from 10 to 12 Å cutoff, and the particle-mesh Ewald method was used to treat long-range electrostatic interactions (60).

Only eight water molecules in the channel pore were extracted from the MD simulation with the symmetric gA dimer from OS ssNMR (1MAG) as the initial structure for quantum chemical calculations. The ONIOM method (61) was used due to the relatively large system. The inner layer with all backbone atoms and water molecules was treated by DFT B3LYP/6-31G(d,p) in geometry optimization. The outer layer with all side chain atoms was treated by universal force field (62) and fixed in the optimization. After optimization, NMR parameters were calculated by the gauge-independent atomic orbital method (63) with the inner layer treated by B3LYP/6-311++G(2d,p).

Data Availability. The data utilized in this manuscript to justify the results and conclusions of this work are entirely presented within the manuscript.

ACKNOWLEDGMENTS. This work was supported in part by NIH Grants AI023007, AI119178, GM122698, and GM118091, and the Pukyong National University Research Abroad Fund in 2017(C-D-2017-0984). The 35.2 T magnet and spectrometer were supported by NSF Grants DMR-1039938 and DMR-0603042. The NMR experiments were performed at the National High Magnetic Field Laboratory, funded by the NSF Division of Materials Research (DMR-1644779) and the State of Florida.

1. A. M. Klibanov, Enzymatic catalysis in anhydrous organic solvents. *Trends Biochem. Sci.* **14**, 141–144 (1989).
2. D. J. Tobias, J. E. Mertz, C. L. Brooks, 3rd, Nanosecond time scale folding dynamics of a pentapeptide in water. *Biochemistry* **30**, 6054–6058 (1991).
3. F. Xu, T. A. Cross, Water: Foldase activity in catalyzing polypeptide conformational rearrangements. *Proc. Natl. Acad. Sci. U.S.A.* **96**, 9057–9061 (1999).
4. R. Barnes et al., Spatially heterogeneous surface water diffusivity around structured protein surfaces at equilibrium. *J. Am. Chem. Soc.* **139**, 17890–17901 (2017).
5. M.-C. Bellissent-Funel et al., Water determines the structure and dynamics of proteins. *Chem. Rev.* **116**, 7673–7697 (2016).
6. A. Horner, P. Pohl, Single-file transport of water through membrane channels. *Faraday Discuss.* **209**, 9–33 (2018).
7. D. F. Savage, P. F. Egea, Y. Robles-Colmenares, J. D. O'Connell, 3rd, R. M. Stroud, Architecture and selectivity in aquaporins: 2.5 Å X-ray structure of aquaporin Z. *PLoS Biol.* **1**, E72 (2003).
8. S. M. Saparov, P. Pohl, Beyond the diffusion limit: Water flow through the empty bacterial potassium channel. *Proc. Natl. Acad. Sci. U.S.A.* **101**, 4805–4809 (2004).
9. M. Weingarth et al., Quantitative analysis of the water occupancy around the selectivity filter of a K^+ channel in different gating modes. *J. Am. Chem. Soc.* **136**, 2000–2007 (2014).

10. O. S. Andersen, Ion movement through gramicidin A channels. Single-channel measurements at very high potentials. *Biophys. J.* **41**, 119–133 (1983).
11. G. Hummer, J. C. Rasaiah, J. P. Noworyta, Water conduction through the hydrophobic channel of a carbon nanotube. *Nature* **414**, 188–190 (2001).
12. I. Kocsis *et al.*, Oriented chiral water wires in artificial transmembrane channels. *Sci. Adv.* **4**, eaao5603 (2018).
13. M. Barboiu *et al.*, An artificial primitive mimic of the Gramicidin-A channel. *Nat. Commun.* **5**, 4142 (2014).
14. R. B. Little, R. J. Dubos, R. D. Hotchkiss, Action of gramicidin on streptococci of bovine mastitis. *Proc. Soc. Exp. Biol. Med.* **44**, 444–445 (1940).
15. E. Genée, C. Schlechtweg, P. Bauerreiss, J. R. R. Gibson, Trimethoprim-polymyxin eye drops versus neomycin-polymyxin-gramicidin eye drops in the treatment of presumptive bacterial conjunctivitis - a double-blind study. *Ophthalmologica* **184**, 92–96 (1982).
16. R. R. Ketchem, W. Hu, T. A. Cross, High-resolution conformation of gramicidin A in a lipid bilayer by solid-state NMR. *Science* **261**, 1457–1460 (1993).
17. R. Ketchem, B. Roux, T. Cross, High-resolution polypeptide structure in a lamellar phase lipid environment from solid state NMR derived orientational constraints. *Structure* **5**, 1655–1669 (1997).
18. A. L. Lomize, V. Iu. Orekhov, A. S. Arsen'ev, [Refinement of the spatial structure of the gramicidin A ion channel] [in Russian]. *Bioorg. Khim.* **18**, 182–200 (1992).
19. L. E. Townsley, W. A. Tucker, S. Sham, J. F. Hinton, Structures of gramicidins A, B, and C incorporated into sodium dodecyl sulfate micelles. *Biochemistry* **40**, 11676–11686 (2001).
20. R. Fu, M. Cotten, T. A. Cross, Inter- and intramolecular distance measurements by solid-state MAS NMR: Determination of gramicidin A channel dimer structure in hydrated phospholipid bilayers. *J. Biomol. NMR* **16**, 261–268 (2000).
21. F. Tian, T. A. Cross, Cation transport: An example of structural based selectivity. *J. Mol. Biol.* **285**, 1993–2003 (1999).
22. V. Lemaître *et al.*, Solid-state ^{17}O NMR as a probe for structural studies of proteins in biomembranes. *J. Am. Chem. Soc.* **126**, 15320–15321 (2004).
23. B. Valentine *et al.*, Oxygen- 17 n.m.r. of peptides. *Int. J. Pept. Protein Res.* **25**, 56–68 (1985).
24. J. Hu *et al.*, Ion solvation by channel carbonyls characterized by ^{17}O solid-state NMR at 21 T. *J. Am. Chem. Soc.* **127**, 11922–11923 (2005).
25. J. Zhu, E. Ye, V. Tersikh, G. Wu, Solid-state (^{17}O) NMR spectroscopy of large protein-ligand complexes. *Angew. Chem. Int. Ed. Engl.* **49**, 8399–8402 (2010).
26. A. W. Tang, X. Kong, V. Tersikh, G. Wu, Solid-state ^{17}O NMR of unstable Acyl-enzyme intermediates: A direct probe of hydrogen bonding interactions in the oxyanion hole of serine proteases. *J. Phys. Chem. B* **120**, 11142–11150 (2016).
27. E. G. Keeler, V. K. Michaelis, R. G. Griffin, (^{17}O) NMR investigation of water structure and dynamics. *J. Phys. Chem. B* **120**, 7851–7858 (2016).
28. R. P. Young *et al.*, Solution-state (^{17}O) Quadrupole central-transition NMR spectroscopy in the active site of tryptophan synthase. *Angew. Chem. Int. Ed. Engl.* **55**, 1350–1354 (2016).
29. A. Wong, F. Poli, "Chapter three - solid-state ^{17}O NMR studies of biomolecules" in *Annual Reports on NMR Spectroscopy*, G. A. Webb, Ed. (Academic Press, 2014), vol. 83, pp. 145–220.
30. T. H. Sefzik *et al.*, Solid-state ^{17}O NMR in carbohydrates. *Chem. Phys. Lett.* **434**, 312–315 (2007).
31. E. G. Keeler *et al.*, ^{17}O MAS NMR Correlation spectroscopy at high magnetic fields. *J. Am. Chem. Soc.* **139**, 17953–17963 (2017).
32. E. A. Chekmenev, J. Paulino, R. Fu, T. A. Cross, "Anisotropic and isotropic chemical shifts perturbations from solid state NMR spectroscopy for structural and functional Biology" in *Modern Magnetic Resonance*, G. A. Webb, Ed. (Springer International Publishing, Cham, 2018), pp. 505–519.
33. I. C. M. Kwan, X. Mo, G. Wu, Probing hydrogen bonding and ion-carbonyl interactions by solid-state ^{17}O NMR spectroscopy: G-Ribbon and G-quartet. *J. Am. Chem. Soc.* **129**, 2398–2407 (2007).
34. E. Y. Chekmenev, P. L. Gor'kov, T. A. Cross, A. M. Alaouie, A. I. Smirnov, Flow-through lipid nanotube arrays for structure-function studies of membrane proteins by solid-state NMR spectroscopy. *Biophys. J.* **91**, 3076–3084 (2006).
35. R. R. Ketchem, K. C. Lee, S. Huo, T. A. Cross, Macromolecular structural elucidation with solid-state NMR-derived orientational constraints. *J. Biomol. NMR* **8**, 1–14 (1996).
36. Z. Gan *et al.*, NMR spectroscopy up to 35.2T using a series-connected hybrid magnet. *J. Magn. Reson.* **284**, 125–136 (2017).
37. W. Mai, W. Hu, C. Wang, T. A. Cross, Orientational constraints as three-dimensional structural constraints from chemical shift anisotropy: The polypeptide backbone of gramicidin A in a lipid bilayer. *Protein Sci.* **2**, 532–542 (1993).
38. D. Massiot *et al.*, Towards higher resolution for quadrupolar nuclei in solid state NMR at very high field. *Comptes Rendus Acad. Sci. Series IIC-Chemistry* **1**, 157–162 (1998).
39. Z. Gan, P. Gor'kov, T. A. Cross, A. Samoson, D. Massiot, Seeking higher resolution and sensitivity for NMR of quadrupolar nuclei at ultrahigh magnetic fields. *J. Am. Chem. Soc.* **124**, 5634–5635 (2002).
40. Y. Chen, A. Tucker, B. A. Wallace, Solution structure of a parallel left-handed double-helical gramicidin-A determined by 2D ^1H NMR. *J. Mol. Biol.* **264**, 757–769 (1996).
41. B. M. Burkhardt, N. Li, D. A. Langs, W. A. Pangborn, W. L. Duax, The conducting form of gramicidin A is a right-handed double-stranded double helix. *Proc. Natl. Acad. Sci. U.S.A.* **95**, 12950–12955 (1998).
42. N. Höfer, D. Aragão, M. Caffrey, Crystallizing transmembrane peptides in lipidic mesophases. *Biophys. J.* **99**, L23–L25 (2010).
43. R. Pomès, B. Roux, Structure and dynamics of a proton wire: A theoretical study of H⁺ translocation along the single-file water chain in the gramicidin A channel. *Biophys. J.* **71**, 19–39 (1996).
44. S. W. Chiu, S. Subramaniam, E. Jakobsson, J. A. McCammon, Water and polypeptide conformations in the gramicidin channel. A molecular dynamics study. *Biophys. J.* **56**, 253–261 (1989).
45. J. Lu *et al.*, Solid-state ^{17}O NMR reveals hydrogen-bonding energetics: Not all low-barrier hydrogen bonds are strong. *Angew. Chem. Int. Ed. Engl.* **56**, 6166–6170 (2017).
46. A. Wong *et al.*, Experimental and theoretical ^{17}O NMR study of the influence of hydrogen-bonding on C=O and O-H oxygens in carboxylic solids. *J. Phys. Chem.* **110**, 1824–1835 (2006).
47. D. W. Boykin, A. Kumar, ^{17}O NMR spectroscopy: Intramolecular hydrogen bonding in 7 hydroxyindanones. *J. Mol. Struct.* **298**, 121–127 (1993).
48. X. Kong *et al.*, Variable-temperature ^{17}O NMR studies allow quantitative evaluation of molecular dynamics in organic solids. *J. Am. Chem. Soc.* **134**, 14609–14617 (2012).
49. F. G. Vogt, H. Yin, R. G. Forcino, L. Wu, ^{17}O solid-state NMR as a sensitive probe of hydrogen bonding in crystalline and amorphous solid forms of diflunisal. *Mol. Pharm.* **10**, 3433–3446 (2013).
50. A. Muralidharan, L. R. Pratt, M. I. Chaudhari, S. B. Rempe, Quasi-chemical theory for anion hydration and specific ion effects: Cl⁻(aq) vs. Fl⁻(aq). *Chem. Phys. Lett.* **X 4**, 100037 (2019).
51. B. W. Urban, S. B. Hladky, D. A. Haydon, Ion movements in gramicidin pores. An example of single-file transport. *Biochim. Biophys. Acta* **602**, 331–354 (1980).
52. O. S. Andersen, Ion movement through gramicidin A ion channels. Studies on the diffusion-controlled association step. *Biophys. J.* **41**, 147–165 (1983).
53. A. Steinschneider, M. I. Bugar, A. Buku, D. Fiat, Labeling of amino acids and peptides with isotopic oxygen as followed by ^{17}O -N.M.R. *Int. J. Pept. Protein Res.* **18**, 324–333 (1981).
54. P. V. LoGrasso, F. Moll, 3rd, T. A. Cross, Solvent history dependence of gramicidin A conformations in hydrated lipid bilayers. *Biophys. J.* **54**, 259–267 (1988).
55. I. Altan, D. Fusco, P. V. Afonine, P. Charbonneau, Learning about biomolecular solvation from water in protein crystals. *J. Phys. Chem. B* **122**, 2475–2486 (2018).
56. A. P. M. Kentgens, R. Verhagen, Advantages of double frequency sweeps in static, MAS and MQMAS NMR of spin $I=3/2$ nuclei. *Chem. Phys. Lett.* **300**, 435–443 (1999).
57. J. C. Phillips *et al.*, Scalable molecular dynamics with NAMD. *J. Comput. Chem.* **26**, 1781–1802 (2005).
58. J. Huang *et al.*, CHARMM36m: An improved force field for folded and intrinsically disordered proteins. *Nat. Methods* **14**, 71–73 (2017).
59. W. L. Jorgensen, J. Chandrasekhar, J. D. Madura, R. W. Impey, M. L. Klein, Comparison of simple potential functions for simulating liquid water. *J. Chem. Phys.* **79**, 926–935 (1983).
60. A. Toukaj, C. Sagu, J. Board, T. Darden, Efficient particle-mesh Ewald based approach to fixed and induced dipolar interactions. *J. Chem. Phys.* **113**, 10913–10927 (2000).
61. S. Dapprich, I. Komáromi, K. S. Byun, K. Morokuma, M. J. Frisch, A new ONIOM implementation in Gaussian98. Part I. The calculation of energies, gradients, vibrational frequencies and electric field derivatives. *J. Mol. Struct. THEOCHEM* **461-462**, 1–21 (1999).
62. A. K. Rappe, C. J. Casewit, K. S. Colwell, W. A. Goddard, W. M. Skiff, UFF, a full periodic table force field for molecular mechanics and molecular dynamics simulations. *J. Am. Chem. Soc.* **114**, 10024–10035 (1992).
63. K. Wolinski, J. F. Hinton, P. Pulay, Efficient implementation of the gauge-independent atomic orbital method for NMR chemical shift calculations. *J. Am. Chem. Soc.* **112**, 8251–8260 (1990).